RSC Advances

PAPER

View Article Online
View Journal | View Issue

Cite this: *RSC Adv.*, 2026, **16**, 7459

Greener hydrocarbons: maximizing efficiency in the electro-catalytic upgrading of *n*-caproic acid to renewable fuels

Shaoqin Xu,†[ab] Xiwen Jia,†[ab] Ting Wang,[ab] Ying Guo,[ab] Wenwen Zhang,[ab] Minghan Yin,[ab] Fei Kong,[ab] Lefei Jiao,[ab] Yue Cen,[c] Tinghong Ming *[ab] and Jiajie Xu *[ab]

The industrial-scale microbial conversion of waste carbon into medium-chain carboxylic acids (MCCAs) has become feasible, and their subsequent utilization for hydrocarbon production *via* the Kolbe reaction as a bioenergy source represents a highly promising route. However, controlling the concentrations of MCCAs, pH, and electrode potential during the coupling of these reactions to ensure efficient elongation and improve Kolbe reaction efficiency is crucial for reducing bioenergy production costs. Our study demonstrated that the Kolbe electrolysis of *n*-caproic acid exhibits a concentration threshold of 800 mM; beyond this concentration, the Faraday efficiency stabilizes, reaching a peak of 51.2%. The Kolbe electrolysis at higher substrate concentration could reduce the energy consumption required to produce the same amount of biofuel by approximately 87%. Both acidic and neutral conditions effectively promote the Kolbe reaction. In terms of electrode potential regulation, a voltage of 3.5 V generally yields better electrolysis results.

Received 19th November 2025
Accepted 28th January 2026

DOI: 10.1039/d5ra08929h

rsc.li/rsc-advances

1 Introduction

Over the past 50 years, the world's energy consumption has been continuously increasing. The petroleum consumption had increased to 756 million tons in 2024, with a year-on-year growth of approximately 9.1%.[1] Nevertheless, fossil fuels are non-renewable, and their use is constrained by extraction capacity and finite reserves. Therefore, there is an urgent need to develop alternative energy sources or produce more energy substances to address the scarcity of conventional fossil fuels and mitigate their environmental and climate impacts.[2] In recent years, the development of technologies for the production of renewable chemicals and liquid fuels from sustainable resources has attracted considerable attention in both academia and industry.

Amid recent advances in microbial production of medium-chain carboxylic acids (MCCAs) from waste carbon, Xu *et al.*[3] developed a temperature-phased anaerobic fermentation process, in which acid whey was first converted to lactic acid by a thermophilic *Lactobacillus*-dominated microbiome and subsequently upgraded to MCCAs *via* chain elongation under mesophilic conditions, achieving a maximum *n*-caproic acid production rate of 81 mmol C L^{-1} day^{-1}. The resulting *n*-caproic acid was recovered by continuous liquid–liquid extraction and retained in extraction solution (Fig. 1A).[4] The MCCAs in the extraction solution serve as substrates for Kolbe electrolysis (carboxylic acid electrolysis) to generate hydrocarbon with phase separation (Fig. 1). Although low acid concentrations and alkaline conditions favour liquid–liquid extraction selectivity,[5] they are not optimal for Kolbe electrolysis. Therefore, elucidating the effects of MCCA concentration and pH in the extraction solution on the efficiency and energy consumption of the Kolbe reaction provides essential data support for integrating liquid–liquid extraction to improve overall process and energy efficiency, as well as for the subsequent utilization of the gaseous by-products (*e.g.*, H_2, CO_2, and O_2, Fig. 1B and C) generated.

Recent research on Kolbe electrolysis has focused on key areas including electrode material selection, the use of supporting electrolytes, optimization of electrolyte flow rate, and reactor design improvements.[6] However, critical parameters such as electrolyte concentration, electrode potential, and pH remain insufficiently studied. Among these, the concentration of MCCAs plays a critical and dual role: as a product, it modulates microbial chain elongation efficiency and associated toxicity, while as a substrate, it dictates the rate of the Kolbe electrolysis reaction.[7,8] Therefore, maintaining a balanced concentration of MCCAs is essential to ensure the efficient extraction efficiency and the subsequent formation of

[a]*School of Marine Science, Ningbo University, Ningbo, Zhejiang, China. E-mail: mingtinghong@nbu.edu.cn; xujiajie@nbu.edu.cn*

[b]*Microbial Development and Metabolic Engineering Laboratory, Ningbo University, Ningbo, Zhejiang, China*

[c]*The Village School, Whittington Drive Houston, TX 77077, USA*

† These authors contributed equally to this work.

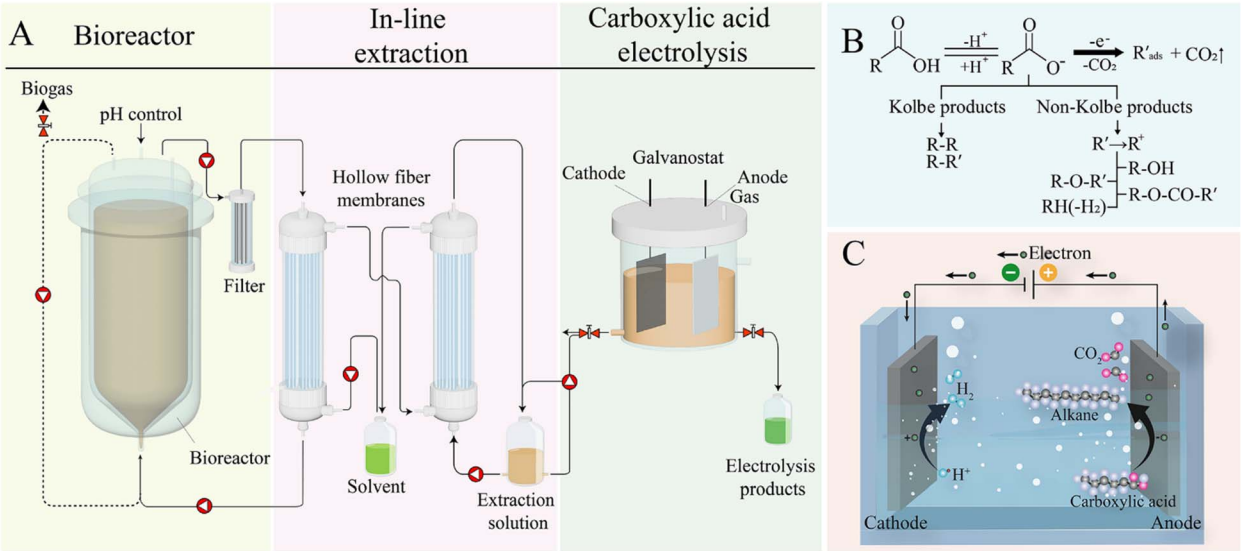

Fig. 1 Schematic representation of the integrated bioprocess-electrolysis system for *in situ* conversion of biogenic carboxylic acids into biofuels. (A) Bioreactor with pH-controlled fermentation coupled to in-line extraction through hollow-fiber membranes,[3,4] where the extraction solution is subsequently directed to the Kolbe electrochemical reactor for biofuel production (Fig. S1 and S2). (B) Kolbe and non-Kolbe electrolysis pathways showing oxidative decarboxylation and product formation. (C) Electrolysis cell illustrating electron transfer and the generation of alkanes, CO_2, H_2 and O_2.

downstream alkane products. Moreover, pH in the extraction significantly impacts liquid–liquid extraction efficiency, microbial activity, equipment corrosion.[9] Thus, understanding the effect of pH on Kolbe electrolysis impacts on the efficiency of microbial fuel production system.

This study employed *n*-caproic acid—a widely studied MCCAs in biomass energy research—as the substrate for Kolbe electrolysis, examining the effects of its concentration, electrolysis potential, and pH on the process. Meanwhile, we developed a sealed Kolbe electrolysis device (Fig. S1) to accurately measure the yield and composition of the generated gases, providing data support for their subsequent utilization. By analyzing the multi-dimensional data, the optimal conditions for *n*-caproic acid Kolbe electrolysis in a platinum electrode system were derived, providing key guidance for both academic research and engineering applications.

2 Materials and methods

2.1 Materials

All chemical reagents used are of analytical grade or above. All solutions are diluted or dissolved with deionized water of the same type. *n*-Caproic acid (99%), *n*-hexane (for dilution, 95%), *n*-decane (analytical standard, 99.5%), sodium hydroxide (for adjusting pH), absolute ethanol (95%), formic acid (99%). Further chemicals used as analytical standards such as acetic acid (0.01 M), propionic acid (0.01 mM), isobutyric acid (0.01 mM), butyric acid (0.01 M), isovaleric acid (0.01 M), valeric acid (0.01 M), isocaproic acid (0.01 M), *n*-caproic acid (0.01 M) and *n*-heptanoic acid (0.01 M), were purchased from Thermo Fisher Scientific, Inc. (Waltham, MA, USA).

2.2 Electrode selection

Platinum (Pt) electrodes are favorable for the single-electron oxidation of carboxylate ions, leading to the formation of alkyl radicals. Owing to their weak adsorption affinity toward radical intermediates, the generated radicals readily desorb from the electrode surface and undergo coupling reactions in the solution phase. This characteristic effectively promotes the Kolbe reaction pathway while suppressing Hofer–Moest type secondary oxidation processes.[10] Accordingly, a Pt plate (10 × 10 × 0.1 mm) was employed as the working electrode, while a titanium plate of identical dimensions was used as the counter electrode, and an Ag/AgCl electrode served as the reference electrode.

2.3 Electrode cleaning

To remove surface oxides that may form on the electrodes during electrolysis, a standardized ultrasonic cleaning procedure was applied after each experiment. Specifically, the electrodes were ultrasonically cleaned in anhydrous ethanol for 15 min, followed by ultrasonic cleaning in deionized water for an additional 15 min.

2.4 Electrochemical tests

The electrochemical experiments were conducted in a 100 mL five-hole electrolytic cell (Fig. S1). The anode and cathode were secured using polytetrafluoroethylene sealing plugs. A reference electrode was connected *via* a Luggin capillary (salt bridge) to minimize the electrolyte contamination. During Kolbe electrolysis, gases produced by electrolysis were collected using a Teflon-lined hose, and stored in a dedicated Teflon gas sampling bag (BKMAM Biotech). Prior to electrochemical

Table 1 Experimental data parameters of *n*-caproic acid at different concentrations after 1.00 FE of electrolysis ($n = 3$)

	Concentrations (mM)										
Parameters	50	100	200	300	400	500	600	700	800	1000	1500
Input charge number (C)	482.43	964.85	1929.70	2894.55	3859.40	4824.25	5789.10	6753.95	7718.80	9648.50	14 472.75
Electrolysis time (s)	28 988	21 552	21 370	21 894	24 986	26 968	27 373	27 194	28 884	29 835	32 261
Electric energy consumption (Wh)	0.47	0.94	1.88	2.81	3.75	4.68	5.62	6.57	7.51	9.38	14.08
iR (V)	0.58	0.72	0.9	0.64	0.68	0.70	0.78	0.66	0.73	0.78	0.96
Average current densities (mA mm^{-2})	0.09	0.24	0.46	0.73	0.78	0.90	1.06	1.25	1.34	1.62	2.26
n-Decane production (mg)	11.74	64.78	194.27	349.99	599.89	990.43	1371.14	1709.40	2905.02	3297.73	5501.33
Consumption of *n*-caproic acid (mg)	203.45	540.20	1775.00	1902.14	2540.98	3739.16	4117.67	5336.33	6337.74	6801.97	12 009.47
Amount of *n*-decane produced per unit of electric energy (g kWh^{-1})	24.98	64.91	103.34	124.55	159.97	211.63	243.98	260.18	386.82	351.57	390.72
S_{decane} (%)	5.79	11.13	10.96	18.40	23.65	26.52	33.45	32.02	45.85	48.36	45.99
Faradaic efficiency (%)	3.3	8.6	13.7	16.4	21.1	27.9	32.2	34.4	51.2	46.4	51.7
Coulombic efficiency (%)	35.03	46.50	76.40	54.58	54.69	64.38	59.08	65.63	68.20	58.56	—
Carbon balance (%)	—	—	—	—	—	37.59	47.25	45.67	65.77	70.66	62.33
Total amount of generated gas (mL)	—	—	—	—	—	552.89	797.41	914.13	1737.10	2208.15	—
H_2 (mL, %)	—	—	—	—	—	343.34 (62.10%)	561.52 (70.41%)	601.24 (65.77%)	1081.12 (62.24%)	1308.08 (59.24%)	—
O_2 (mL, %)	—	—	—	—	—	26.57 (4.81%)	10.83 (1.36%)	17.98 (1.97%)	15.88 (0.91%)	23.42 (1.06%)	—
CO_2 (mL, %)	—	—	—	—	—	73.31 (13.26%)	100.56 (12.61%)	140.25 (15.34%)	272.10 (15.66%)	402.87 (18.24%)	—

experiments, the pH meter was systematically calibrated with standard buffer solutions (pH = 4.01, 7.01 and 9.80) following manufacturer protocols. The electrochemical experiments were performed using a multi-channel electrochemical workstation (Bio-Logic VMP-300, France) with 10 independent channels capable of simultaneous potentiostatic control.

Electrochemical impedance spectroscopy (EIS) measurements were carried out using a conventional three-electrode configuration, consisting of a Pt working electrode, a Pt (or Ti) counter electrode, and an Ag/AgCl reference electrode. Prior to each measurement, the electrochemical cell was allowed to stabilize at open-circuit potential (OCP) for at least 5 min to ensure a steady electrochemical state. EIS spectra were recorded at the OCP by applying a sinusoidal AC perturbation with an amplitude of 5 mV. The frequency range was restricted to the high-frequency region from 1 kHz to 50 kHz, as the primary purpose of the EIS measurements in this study was to determine the solution resistance (R_s) for *iR* correction. Low-frequency processes related to charge transfer and mass transport were therefore not investigated. The impedance data were presented in Nyquist plots, and the R_s was obtained from the high-frequency intercept on the real axis. All measurements were repeated at least three times to ensure reproducibility.

2.5 Influence of concentration on the Kolbe electrolysis

A series of *n*-caproic acid solutions with a volume of 500 mL were prepared at different concentrations, as detailed in Table 1. For the electrolysis electrolyte, no additional supporting compounds other than *n*-caproic acid were introduced, in which *n*-caproic acid was served as both the reactant and the electrolyte. The pH of each solution was adjusted to 6.8–7.1 by titration with 3 M solution NaOH. Subsequently, 100 mL of the electrolyte was accurately measured using a volumetric flask and transferred into the electrochemical cell. Electrolysis experiments were then conducted under identical Faraday equivalent (FE) conditions at a constant voltage of 3.5 V, with the corresponding charge input (Q) required for each electrolyte concentration at different FEs summarized in Table S1.

2.6 Influence of pH variation on the Kolbe electrolysis

To investigate the effect of pH on the Kolbe reaction, *n*-caproic acid electrolytes were prepared and adjusted to three pH levels (5.86, 6.92, and 9.60) using NaOH solution. The electrolysis was controlled by constant potential with a voltage of +3.5 V *vs.* Ag/AgCl sat. (Fig. S3). The selection and treatment of electrodes can refer to the Sections 2.2 and 2.3. In view of the problem of organic phase loss caused by frequent sampling during batch electrolysis (including the escape of volatile components and the disturbance of the liquid–liquid interface), this study optimized the measurement method of faradaic efficiency (FEff). Specifically, the continuous electrolysis mode was adopted. After inputting the full charge amount of 1.00 FE in a closed electrolytic cell, the *n*-decane in the organic phase was directly quantitatively analyzed. By eliminating the systematic errors introduced by intermittent sampling, this method ensured the product recovery rate and significantly improved the calculation accuracy of FEff.

2.7 Influence of potential level on the Kolbe electrolysis

The input potential exerts a significant influence on the electrochemical reaction. The synergistic mechanism between the electrode potential and the current density decisively impacts the efficiency of the Kolbe electrolysis, as presented in Fig. S4. Ideal operation requires maintaining an optimal current density to balance mass transfer rate and charge transfer efficiency.[11,12] However, achieving stable constant current operation is challenging in practice due to spatiotemporal heterogeneity in electrode polarization effects and concentration overpotential. Furthermore, accurately calculating the electrical energy consumption under constant current mode is difficult. Therefore, this study employed a constant potential operation strategy. Three distinct potential values, all significantly above the critical potential for the Kolbe reaction (2.4 V *vs.* Ag/AgCl), were selected to ensure the dominance of the Kolbe dimerization pathway and to systematically investigate the effect of applied potential. Electrolysis of the electrolyte—an 800 mM *n*-caproic acid solution at pH 6.92 was performed until a charge corresponding to 1.00 FE was passed at each potential.

2.8 Analysis of the electrochemical products

2.8.1 Aqueous phase. After completion of the experiments, the collected samples were diluted. The diluted samples were acidified with 5% formic acid, filtered through a 0.22 μm membrane filter, and then transferred into 2 mL Agilent vials for gas chromatography (GC) analysis. GC analysis was performed using an Agilent 7890A system equipped with a flame ionization detector (FID). Separation was achieved on a DB-FFAP capillary column (30 m × 250 μm ID, 0.25 μm film thickness; Agilent, Santa Clara, USA), with nitrogen used as the carrier gas at a constant flow rate of 1.5 mL min^{-1}. The injector temperature was maintained at 240 °C, and a split ratio of 30 : 1 was applied. The column oven temperature program was as follows: the initial temperature was held at 80 °C for 1 min, ramped to 115 °C at 15 °C min^{-1} and held for 3 min, then increased to 130 °C at 3 °C min^{-1}, followed by a final ramp to 230 °C at 15 °C min^{-1}. The FID detector temperature was maintained at 300 °C.

Carboxylic acids (CAs) were identified and quantified using the external standard method. The retention times of individual CAs were calibrated using fatty acid standard mixtures. Quantitative analysis was conducted based on peak areas, and the concentration profiles of CAs were subsequently used to calculate the coulombic efficiency (CE) of *n*-caproic acid.

2.8.2 Organic phase. First, 10 mL of *n*-hexane was added to the electrolytic cell. The mixture was stirred using a magnetic stirrer for 5 min and then allowed to stand for 10 min. After the solution became homogeneous and stable, 1 mL of the upper organic phase was withdrawn using a disposable syringe, filtered through a 0.22 μm organic membrane filter, and transferred into a 2 mL vial for gas chromatography-mass spectrometry (GC-MS) analysis. Subsequently, an additional

5 mL of *n*-hexane was added to the electrolytic cell, followed by stirring for 5 min and standing for 10 min. Then, 1 mL of the upper clear organic phase was collected for GC-MS analysis. GC-MS analysis was performed using an Anyeep 7700 GC-MS system (Suzhou, China). Separation was achieved on an HP-5MS UI capillary column (30 m × 0.25 mm ID, 0.25 μm film thickness; Agilent, Santa Clara, USA), with helium used as the carrier gas at a constant flow rate of 1.0 mL min^{-1}. The injector temperature was set at 250 °C, with an injection volume of 0.2 μL and a split ratio of 60 : 1. The column oven temperature program was as follows: the initial temperature was set at 50 °C and held for 2 min, then increased to 60 °C at a rate of 2 °C min^{-1}, followed by a ramp to 200 °C at 50 °C min^{-1}, and finally increased to 280 °C at 60 °C min^{-1}. The mass spectrometer was operated with an ion source temperature of 240 °C and a transfer line temperature of 250 °C. Selected ion monitoring was conducted using characteristic *m*/*z* fragments of 57.1, 71.1, and 85.2.

2.8.3 Gas detection. For gas-phase product analysis, a curved gas outlet interface was connected to a Teflon-lined hose, and a Teflon gas collection bag was attached to the other end. After completion of electrolysis at a total charge of 1.00 FE, the collected gas was analyzed by gas chromatography. The instrument used for the analysis is an Anyeep 7700 gas chromatograph analyzer equipped with a TCD (Thermal Conductivity Detector), and argon (Ar) is used as the carrier gas. The GC measurement conditions are as follows: the temperature of the injection port is 250 °C, a 1 μL quantitative valve is configured, the detection temperature of the TCD is 250 °C, the temperature of the valve box is 80 °C, the temperature of the independent small valve box is 100 °C, and the temperature of the chromatographic column is set at 90 °C and maintained for 13 min at a constant temperature. Since the thermal conductivity coefficients of Ar and CO_2 are too close, the measurement of the CO_2 content is inaccurate during gas phase detection. Following the analysis of other gas components, the CO_2 concentration was finally determined using a dedicated CO_2 detector. The CO_2 detector uses a smart carbon dioxide module (SGA-700 series, Shenguoan, Shenzhen). The calibration procedure for the CO_2 detector is described in detail in the SI.

2.9 Data processing and calculation

2.9.1 Ionization of molecules. When preparing the *n*-caproic acid solution, the ionic distribution in the solution was estimated based on the Henderson–Hasselbalch equation.[13] The relationship between the distribution of dissociated carboxylic acid (A^-) and undissociated carboxylic acid (HA) molecules in the aqueous solution and pH was calculated according to eqn (1) and (2).[14]

$$\mathrm{pH} = \mathrm{p}K_a + \log_{10}\left(\frac{C_{(A^-)}}{C_{(HA)}}\right) \quad (1)$$

$$C_i = C_{(A^-)} + C_{(HA)} \quad (2)$$

where $C_{(A^-)}$ represents the concentration of the corresponding carboxylate ion, ($C_{(HA)}$) is the concentration of the CA molecule form, and $C_{(i)}$ is the total concentration of the CA containing this carbon atom in the solution. Consequently, eqn (1) and (2) can be joined to give eqn (3) which gives the concentration of dissociated CA molecules in dependence of the pH. Relating $C_{(A^-)}$ to $C_{(CA)}$ equals the share of dissociated CA molecules:

$$C_{(A^-)} = \frac{C_i \times 10^{(\mathrm{pH}-\mathrm{p}K_a)}}{1 + 10^{(\mathrm{pH}-\mathrm{p}K_a)}} \quad (3)$$

2.9.2 Faraday equivalent. To ensure that the amount of charge input is relatively consistent each time, 1.00 FE is used as the experimental cycle throughout this experiment. FE is defined as the ratio of the charge quantity transferred over time (Q_t) to the charge quantity theoretically required to convert all *n*-caproic acid (Q_{total}), assuming a CE of 100%, and is calculated as follows:[15]

$$\mathrm{FE} = \frac{Q_t}{Q_{total}} = \frac{\int_0^t i\mathrm{d}t}{\sum n_i \times F \times Z} \quad (4)$$

$$Q_{total} = \sum n_i \times F \times Z \quad (5)$$

$$Q_t = \int_0^t i\mathrm{d}t \quad (6)$$

In the equation, n_i represents the amount of substance of *n*-caproic acid, and *Z* denotes the number of electrons transferred per molecule of *n*-caproic acid during the reaction. In the present reaction system, one electron is transferred for each molecule of *n*-caproic acid consumed; therefore, *Z* is taken as 1. The Faraday constant (*F*) is taken as 96 485 C mol^{-1}.

2.9.3 Coulombic efficiency. In this experiment, the CE is used to define the ratio between the amount of electric charge consumed for the oxidation of *n*-caproic acid and the actual input charge as presented in eqn (7).[14]

$$\mathrm{CE} = \frac{Q_i}{Q_t} = \frac{\sum n_{CA\_t} \times F \times Z}{\int_0^t i\mathrm{d}t} \quad (7)$$

In the equation, n_{CA_t} represents the change in the amount of *n*-caproic acid in the aqueous phase of the electrolyte before and after the reaction. This value was determined by GC following appropriate dilution and acidification of the samples.

2.9.4 Faradaic efficiency. In the experiment, we also calculated the FEff of *n*-decane production, which is used to define the ratio between the amount of electric charge required for the production of *n*-decane (Q_{decane}) and the amount of electric charge input (Q_t) as shown in eqn (8):

$$\mathrm{FEff} = \frac{Q_{decane}}{Q_t} = \frac{\sum n_{decane} \times F \times Z}{\int_0^t i\mathrm{d}t} \quad (8)$$

In the formula, n_{decane} refers to the content of *n*-decane in the organic phase of the electrolyte after the reaction, which is determined by GC-MS after dilution. In this reaction system, the number of electrons transferred for the production of 1 molecule of *n*-decane is 2, so $Z = 2$.

2.9.5 Selectivity of electrolysis products. The selectivity of electrolysis products is used to determine the occurrence of the Kolbe electrolysis reaction by calculating the ratio of the amount of substance of *n*-decane produced to that of *n*-caproic acid consumed using the following equation:

$$S_{\text{decane}} = \frac{n_{\text{decane}}}{n_{\text{CA\_t}}} \quad (9)$$

2.9.6 Amount of *n*-decane produced per unit of electrical energy. This item is aimed at evaluating the electrical energy consumption required for the production of *n*-decane using eqn (10) as reported Urban *et al.*[14]

$$E_{\text{decane}} = \frac{m_{\text{decane}}}{W_{\text{we}}} \quad (10)$$

In the formula, m_{decane} represents the mass of *n*-decane measured by GC-MS after the electrolytic reaction is completed. Since the *n*-decane produced comes entirely from the anodic reaction, only the energy consumption of the working electrode, that is W_{we}, needs to be calculated.

2.10 Statistical analysis

All experiments were performed with at least three independent replicates ($n = 3$) for each condition. In this regard independent replicates means that the electrolysis of the *n*-caproic acid solution and the post electrolysis sample preparation and measurement were performed fully independently for each single replicate. All values are given as the mean ± Student *t* confidence interval (CI, $\alpha = 0.05$).

3 Results and discussion

We investigated the reaction coefficients of *n*-caproic acid in Kolbe electrolysis and explored the synergistic effect of concentration on *n*-decane conversion rate and CE using eqn (7). As shown in Fig. 2 and Table S2, the CE decay rate in the 0.50–1.00 FE stage is only 4.82% in the low-concentration (50 mM *n*-caproic acid) system, while the CE decay rate in the high-concentration (800 mM *n*-caproic acid) system is as high as 40.06%. Additionally, when the concentration increases from 50 mM to 700 mM *n*-caproic acid and 0.25 FE is input, the CE surprisingly reaches 96.82 ± 2.70% ($n = 3$), indicating that the charge can be efficiently converted into free radicals within this concentration range. However, when the concentration of *n*-caproic acid reaches to 800 mM, the CE under the same conditions drops to 66.70 ± 9.08%. Within this concentration range.

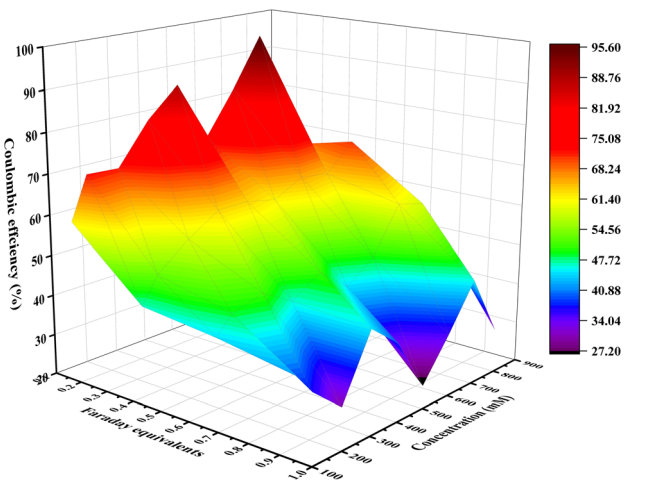

Fig. 2 3D surface plot illustrating the dependence of CE on different Faraday equivalents and concentration (mM) for the Kolbe electrolysis reaction.

Based on the *iR*-corrected electrochemical data and product analysis, a significant increase in FEff was observed with increasing initial caproic acid concentration, indicating that higher substrate concentrations favor electron utilization toward the Kolbe electrolysis reaction. When operated within the *n*-caproic acid concentrations of 50–700 mM under 0.25 FE conditions, the CE exhibited a positive correlation with substrate concentration (Fig. 2), suggesting a surface-controlled process in which the density of electrochemically active sites on the electrode surface constitutes the rate-limiting factor.[16] Further EIS analysis revealed that when the *n*-caproic acid concentration exceeded 800 mM, the *iR* increased markedly (Table 1), indicating a substantial rise in solution. This observation provides quantitative electrochemical evidence for the performance deterioration observed at high substrate concentrations.

Beyond this concentration threshold, the increased resistive losses are likely to contribute to reduced electrolysis efficiency and may be accompanied by mass-transfer limitations.[17] In particular, elevated electrolyte viscosity at high substrate concentrations has been reported to hinder reactant diffusion toward the electrode–electrolyte interface, which could further exacerbate transport limitations under such conditions.[18]

Analysis of the liquid products showed that the carbon was primarily composed of *n*-decane, with a minor fraction of pentyl pentanoate. The abundance of pentyl pentanoate was significantly lower than that of *n*-decane, confirming that *n*-decane is the dominant product in the electrolysis process. The corresponding gas-phase mass spectra are provided in Fig. S5.

The FEff using eqn (8) and product selectivity (S_{decane}, eqn (9)) were determined for the Kolbe electrolysis conducted at a total charge corresponding to 1.00 FE (Fig. 3 and Table 1). As shown in Fig. 3A, the key kinetic parameters showed that within the *n*-caproic acid concentrations from 50 to 800 mM, the FEff showed a significant concentration dependence (from 3.3% to 51.2%), while the consumption of *n*-caproic acid always remained within the range of 48.9–68.8%, without showing significant concentration dependence. This kinetic decoupling phenomenon indicates that when the substrate concentration is lower than 800 mM *n*-caproic acid, the reaction is controlled by the coupling reaction kinetics, and the main reaction occurring in the solution currently is:

$$R - COO^- \xrightarrow{-2e^-} R^{\cdot} \xrightarrow{\text{coupling}} R - R$$

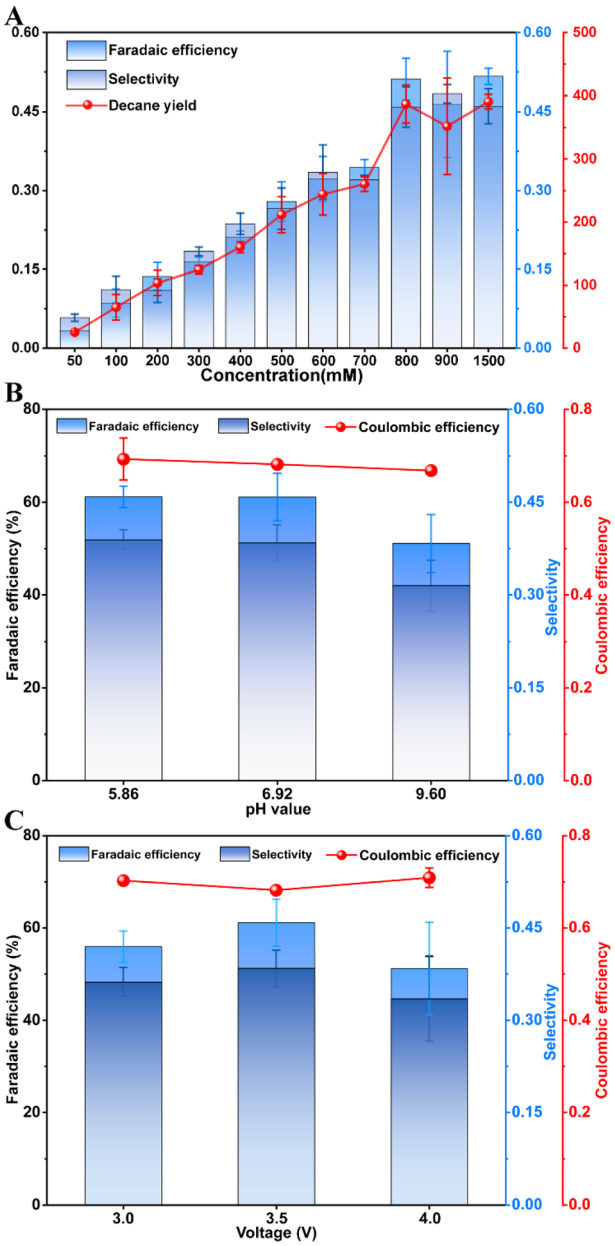

Fig. 3 Comparative analysis of Kolbe electrolysis performance under varying reaction parameters. (A) Effect of initial *n*-caproic acid concentrations on faradaic efficiency (FEff), product selectivity, and *n*-decane yield. (B) Influence of *n*-caproic acid solution pH on FEff, selectivity, and coulombic efficiency (CE). (C) Effect of applied voltage on FEff, selectivity, and CE in the electrolysis of *n*-caproic acid.

When the substrate concentration is higher than 800 mM, the concentration of free radicals exceeds the critical value, and the excessive free radicals begin to be further oxidized into carbocations, resulting in the plateauing of FEff:

$$R^{\cdot} \rightarrow R^{+} \xrightarrow{\text{solvent}} \text{by-products}$$

On this basis, the relationship model between the *n*-caproic acid concentration and the *n*-decane yield/electrical energy efficiency was also considered as shown in Table 1. Since there are significant differences in the input charge amount required for different concentration systems to reach 1.00 FE (50 mM: 0.47 Wh *vs.* 800 mM: 7.51 Wh), the specific energy consumption shows a non-linear evolution pattern. The data shows that within the concentration range of 50–800 mM, the yield per unit of electrical energy (g kWh^{-1}, eqn (10)) increased from 24.98 to 386.82. This indicates that initiating the Kolbe electrolysis at higher substrate concentrations could reduce the energy consumption required to produce the same amount of biofuel by approximately 94%. Previous research on electrocatalytic fuel production has shown that using lower concentrations of *n*-caproic acid (400–500 mM) results in higher energy consumption.[14,19] In contrast, by employing 800 mM *n*-caproic acid in this study, we achieved a notable reduction in energy consumption, from 6.25 or 4.73 Wh g^{-1} to 2.59 Wh g^{-1}. This finding underscores the advantages of optimizing electrolyte concentration for improving energy efficiency in the production of renewable fuels. However, when the concentration of *n*-caproic acid exceeds 800 mM, the selectivity and yield of *n*-decane reach a plateau (Fig. 3A). Specifically, the yields at *n*-caproic acid concentrations of 1000 mM and 1500 mM are 351.57 g kWh^{-1} and 390.72 g kWh^{-1} respectively (Table 1), and this phenomenon is coupled with the FEff stagnation mechanism. This phase change behaviour of the energy-matter conversion efficiency reveals that there is a critical economic concentration window (700–800 mM) in the Kolbe electrolysis process, and increasing the concentration beyond this window cannot achieve energy efficiency gains. The improvement can be attributed to a higher availability of reactive carboxylate ions near the electrode surface, which promotes more efficient electron transfer and suppresses side reactions such as oxygen evolution. Consistent with this observation, our experimental results showed that at the concentration of 500 mM *n*-caproic acid, the oxygen content was 4.81%, whereas in the 600–1000 mM range, the oxygen content decreased markedly to 0.91–1.97% (Table 1), further confirming the suppression of side reactions at higher concentrations.

To evaluate the carbon utilization and validate the reaction pathway, a carbon balance analysis was performed based on the quantified carbon-containing species as described by Neubert *et al.*[20] The carbon input was calculated from the consumed *n*-caproic acid, while the carbon output was determined from the measured *n*-decane in the liquid phase and CO_2 in the gas phase. As shown in Table 1, the majority of the converted carbon was recovered in *n*-decane, confirming that the Kolbe electrolysis pathway dominated under the investigated conditions. Also, CO_2 accounted for a smaller but measurable fraction of the carbon output, consistent with the decarboxylation mechanism of the Kolbe reaction. Besides this, GC-MS analysis of the organic phase revealed that *n*-decane was the predominant liquid product, accompanied by a minor amount of pentyl pentanoate as the main organic by-product (Fig. S5). It should be noted that the apparent carbon recovery obtained in this study did not reach 100%, remaining at approximately 60% under most experimental conditions (Table 1). This incomplete carbon closure may primarily arise from the intrinsic characteristics of Kolbe electrolysis systems as well as experimental

limitations. During anodic decarboxylation, a fraction of carbon is converted into volatile hydrocarbons and radical-derived by-products, which are likely partitioned into the headspace but were not quantitatively analyzed in this study. In addition, although gaseous CO_2 was detected, a substantial portion of the generated CO_2 is expected to dissolve in the electrolyte and therefore could not be fully captured by gas-phase analysis. Minor carbon losses may also originate from incomplete extraction efficiency and the formation of trace oxygenated by-products *via* secondary oxidation pathways; however, the concentrations of these compounds were below the detection limit of GC-MS. Similar observations have been reported in previous studies on Kolbe electrolysis systems.[21]

In addition, in order to elucidate the charge distribution behavior and product selectivity of Kolbe electrolysis under different pH conditions, a series of pH-controlled experiments were conducted at a fixed *n*-caproic acid concentration. The dissociation behavior of *n*-caproic acid was quantitatively evaluated using eqn (1) (the pK_a of *n*-caproic acid is 4.88). As the pH increased from weakly acidic (pH 5.86) to alkaline (pH 6.92) conditions, the proportion of dissociated CAs increased markedly. Specifically, the molar ratio of HA to A^- shifted from approximately 1 : 10 at pH 5.86 to 1 : 110 at pH 6.92 and further to 1 : 52 500 at pH 9.60, indicating a pronounced change in electrolyte speciation. These changes in species speciation were directly reflected in the electrochemical characteristics of the system. *iR* measurements revealed pronounced differences in the ohmic voltage drop among the electrolytes at different pH values (Table S3), indicating that the ohmic energy loss associated with charge transport was effectively minimized at pH 6.92. Correspondingly, under constant-voltage operation at 3.5 V, the system exhibited distinct current responses. The resulting current densities were 119.33 $\pm$ 1.52 mA cm^{-2}, 137.22 $\pm$ 0.35 mA cm^{-2}, and 129.20 $\pm$ 1.15 mA cm^{-2} at pH 5.86, 6.92, and 9.60, respectively (Fig. S3).

Moreover, the effects of pH on the charge distribution, electrochemical efficiency, and product selectivity in Kolbe electrolysis reaction were investigated as depicted in Fig. 3B and Table S3. Although neutral and alkaline conditions provide higher ionic conductivity and enable larger current densities, GC-MS analysis revealed that FEff did not increase accordingly. The alkaline system (pH 9.60) exhibited a significantly lower FEff (44.5 $\pm$ 3.2%) compared with the neutral (pH 6.92, 52.9 $\pm$ 0.1%) and weakly acidic (pH 5.86, 52.5 $\pm$ 1.9%) systems (Fig. 3B). A similar decreasing trend was observed for CE, which declined from 69.3% at pH 5.86 to 68.2% at pH 6.92, and further to 66.85% at pH 9.60. These results indicate that, despite the lower intrinsic solution resistance under neutral and alkaline conditions, a progressively larger fraction of the current was diverted toward parasitic reactions. Consistent with the trends in FEff and CE, the energy-normalized yield of *n*-decane also exhibited a pronounced dependence on pH (Table S3). The *n*-decane yields reached 392.64 g kWh^{-1} at pH 5.86 and 386.82 g kWh^{-1} at pH 6.92, whereas a substantial decrease to 317.01 g kWh^{-1} was observed under alkaline conditions (pH 9.60). These results indicate that, despite the higher current densities achievable under neutral and alkaline conditions, the effective conversion of electrical energy into the target hydrocarbon was most favourable under weakly acidic and neutral environments.

Based on these observations, the present results are in strong agreement with previously reported studies that Kolbe electrolysis achieves optimal efficiency under weakly acidic to neutral pH conditions.[18,22,23] Mechanistically, under alkaline conditions, CAs predominantly exist as carboxylate anions, accompanied by a high concentration of hydroxide ions. Hydroxide ions compete with carboxylate anions for anodic discharge sites and can undergo anodic oxidation to generate oxygen,[24] thereby diverting part of the applied current away from the Kolbe reaction and reducing the effective FEff for target products. Moreover, the increased hydroxide concentration may enhance steric hindrance among alkyl radicals, rendering radical–radical coupling less favorable.[25] Because the Pt electrode is in direct contact with the electrolyte, weakly acidic and neutral environments facilitate the formation of an electrode surface state that favors carboxylate adsorption and electron transfer.[26] In contrast, under alkaline conditions, the excessive presence of hydroxide ions may induce the formation of an alkaline surface layer or trigger surface chemical transformations on the Pt electrode,[27,28] altering surface properties and hindering effective electron transfer. These combined effects ultimately lead to increased *iR* losses, reduced charge utilization efficiency, and a decline in FEff.

Headspace gas analysis showed a slightly higher O_2 content under alkaline conditions (2.53 vol%) than in neutral (0.91 vol%) and weakly acidic (1.05 vol%) systems, but overall O_2 yield remained low (Table S3), consistent with literature reports.[29,30] Notably, CO_2 solubility significantly depends on electrolyte pH, leading to a non-linear relationship between detected gas-phase CO_2 and actual production. Thus, the lower CO_2 proportion under alkaline conditions (12.97 vol% *vs.* 15.66 vol% at pH 6.92 and 22.77 vol% at pH 5.86) mainly reflects higher solubility in basic media rather than lower CO_2 generation.[31] Additionally, alkaline conditions may promote the formation of a hydroxide layer or surface reactions on the electrode, altering its properties and hindering contact between carboxylate ions and the electrode, thereby reducing electron transfer efficiency and FEff.[27]

By testing the Kolbe electrolysis of *n*-caproic acid at anodic potentials from 3.0 to 4.0 V (*vs.* Ag/AgCl), the influence of potential on FEff and selectivity was examined. As shown in Fig. 3C and S4, increasing the anodic potential raised the current density, while *n*-decane selectivity first increased and then decreased. Optimal performance occurred at 3.5 V at our setup, with FEff reaching 52.9 $\pm$ 0.1% and *n*-decane selectivity at 49.5 $\pm$ 1.8%, significantly higher than at 3.0 V or 4.0 V. At 3.0 V, low energy input resulted in insufficient decarboxylation activation energy, limiting radical generation below the coupling threshold and promoting non-Kolbe side reactions.[32,33] At 4.0 V, high energy input accelerated the reaction but caused severe anode polarization, excess radical generation, side reactions, reduced FEff, and Pt electrode oxidation, increasing charge transfer resistance.[34] At 3.5 V, the energy input matched the decarboxylation activation window, enabling efficient charge transfer and high selectivity. This voltage balances high FEff

with reduced energy waste and simplifies product purification, offering valuable guidance for industrial application.

4 Conclusions

The results indicate that Faraday efficiency increased with concentration up to a threshold of 800 mM, beyond which no further improvement occurred. Coulometric efficiency was influenced by both electrode activity and concentration, with an anomalous initial decrease above 700 mM that stabilized after 1.00 FE of charge passed. Acidic and neutral pH conditions were more favourable for high FE than alkaline conditions. Regarding electrode potential, FE initially increased and then decreased, with an optimum at 3.5 V. These findings not only provide critical insights into optimizing the Kolbe electrolysis of caproic acid but also hold significant practical implications. By coupling with microbial chain elongation technologies, the optimized electrolysis parameters can effectively reduce the overall production cost of biofuels derived from renewable feedstocks. Furthermore, the established optimal conditions pave the way for future large-scale process development by enhancing energy efficiency and reducing operational energy consumption.

Author contributions

Shaoqin Xu: writing – original draft, writing – review and editing, data curation, methodology; Xiwen Jia: writing – original draft, data curation, methodology; Ting Wang: methodology, investigation; Ying Guo: methodology, investigation; Wenwen Zhang: writing – original draft, data curation; Minghan Yin: writing – original draft, data curation; Fei Kong: writing – review and editing, investigation; Lefei Jiao: writing – review and editing, investigation; Yue Cen: conceptualization, methodology; Tinghong Ming: writing – original draft, writing – review and editing, data curation, methodology; Jiajie Xu: writing – original draft, data curation, methodology, investigation, supervision.

Conflicts of interest

The authors declare no conflicts of interest.

Data availability

All data supporting the findings of this study are available from the corresponding author upon reasonable request. Supplementary information (SI) is available. See DOI: https://doi.org/10.1039/d5ra08929h.

Acknowledgements

This work was financially supported by the Ningbo Municipal Bureau of Science and Technology (no. 2023H023); Ningbo Innovation "Yongjiang 2035" Key Research and Development Programme (no. 2025Z109); National Natural Science Foundation of China (no. 23FAA01731); School Talent Engineering Project (Management) (no. ZX2023000122); Ningbo Municipal Talent Office (no. ZX2023000069); Department of Science and Technology of Zhejiang Province (no. 2024C03128), and the K.C. Wong Magna Fund in Ningbo University.

Notes and references

1 D. Zhang, M. Zhao, Y. Wang, S. A. Vigne and R. Benkraiem, *Energy Econ.*, 2024, **131**, 107321.
2 L. T. Angenent, I. Casini, U. Schröder, F. Harnisch and B. Molitor, *Energy Environ. Sci.*, 2024, **17**, 3682–3699.
3 J. Xu, J. Hao, J. J. L. Guzman, C. M. Spirito, L. A. Harroff and L. T. Angenent, *Joule*, 2018, **2**, 280–295.
4 J. Xu, B. Bian, L. T. Angenent and P. E. Saikaly, *Front. Bioeng. Biotechnol.*, 2021, **9**, 726946.
5 C. Urban, J. Xu, H. Straeuber, T. R. dos Santos Dantas, J. Muehlenberg, C. Haertig, L. T. Angenent and F. Harnisch, *Energy Environ. Sci.*, 2017, **10**, 2231–2244.
6 K. Neubert, M. Schmidt and F. Harnisch, *ChemSusChem*, 2021, **14**, 3097–3109.
7 M. Zheng, J. Xu, X. Xu, Z. Tang, Y. Hou, X. Li, Q. Li, M. Li, D. Wei and Z. Cao, *Int. J. Electrochem. Sci.*, 2025, **20**, 101091.
8 S. Wang, D. Ren, Y. Du, M. Zhang, N. Zhang, Y. Sun and Z. Huo, *Carbon Resour. Convers.*, 2023, **6**, 287–297.
9 R. Palomo-Briones, J. Xu, C. M. Spirito, J. G. Usack, L. H. Trondsen, J. J. L. Guzman and L. T. Angenent, *Chem. Eng. J.*, 2022, **446**, 137170.
10 D. M. Heard and A. J. J. Lennox, *Angew. Chem., Int. Ed.*, 2020, **59**, 18866–18884.
11 G. Pande and S. Shukla, *Electrochim. Acta*, 1961, **4**, 215–231.
12 H. J. Schäfer, *Eur. J. Lipid Sci. Technol.*, 2012, **114**, 2–9.
13 P. D. Constable, *Vet. Clin. North Am.: Food Anim. Pract.*, 2014, **30**, 295–316.
14 C. Urban, J. Xu, H. Sträuber, T. R. dos Santos Dantas, J. Mühlenberg, C. Härtig, L. T. Angenent and F. Harnisch, *Energy Environ. Sci.*, 2017, **10**, 2231–2244.
15 C. Stang and F. Harnisch, *ChemSusChem*, 2015, **9**, 50–60.
16 B. Qiu, X. Tao, Y. Wang, D. Zhang and H. Chu, *Environ. Chem. Lett.*, 2025, **23**, 81–115.
17 F. J. Holzhäuser, J. B. Mensah and R. J. Palkovits, *Green Chem.*, 2020, **22**, 286–301.
18 H.-J. Schäfer, in *Electrochemistry IV*, Springer, 2005, pp. 91–151.
19 L. F. M. Rosa, K. Röhring and F. Harnisch, *Fuel*, 2024, **356**, 129590.
20 K. Neubert, M. Hell, M. Chávez Morejón and F. Harnisch, *ChemSusChem*, 2022, **15**, e202201426.
21 N. Teetz, D. Holtmann, F. Harnisch and M. Stöckl, *Angew. Chem.*, 2022, **134**, e202210596.
22 J. C. Churchill, PhD thesis, University of York, 2022.
23 D. Seebach and P. Renaud, *Helv. Chim. Acta*, 1985, **68**, 2342–2349.
24 J. Joo, T. Uchida, A. Cuesta, M. T. Koper and M. Osawa, *Electrochim. Acta*, 2014, **129**, 127–136.
25 H. J. Schäfer, *Eur. J. Lipid Sci. Technol.*, 2011, **114**, 2–9.
26 Y. B. Vassiliev and V. A. Grinberg, *J. Electroanal. Chem. Interfacial Electrochem.*, 1991, **308**, 1–16.

27 S. Liu, N. Govindarajan, H. Prats and K. Chan, *Chem Catal.*, 2022, **2**, 1100–1113.
28 E. Artmann, P. V. Menezes, L. Forschner, M. M. Elnagar, L. A. Kibler, T. Jacob and A. K. Engstfeld, *ChemPhysChem*, 2021, **22**, 2429–2441.
29 P. Levy, J. Sanderson and L. Cheng, *J. Electrochem. Soc.*, 1984, **131**, 773.
30 Z. Zeng, A. Feceu, N. Sivendran and L. Gooßen, *Adv. Synth. Catal.*, 2021, **363**, 2678–2722.
31 R. Battino and H. L. Clever, *Chem. Rev.*, 1966, **66**, 395–463.
32 H.-H. Dong, Y.-X. Zhu, Y.-G. Li, J.-Y. Liang, Y. Tan, X.-Y. Zhang, H.-M. Jiang, L. Lin and Z.-M. Sun, *Tungsten*, 2024, **6**, 696–710.
33 Z. Tan, H. Zhang, K. Xu and C. Zeng, *Sci. China: Chem.*, 2023, **67**, 450–470.
34 S. Blank, Z. Nguyen, D. G. Boucher and S. D. Minteer, *Curr. Opin. Electrochem.*, 2022, **35**, 101049.